Journal of Solid State Chemistry **147,** 399–409 (1999)
Article ID jssc.1999.8405, available online at http://www.idealibrary.com on IDEAL®

# Competition between Magnetism and Superconductivity in Erbium Rhodium Stannide

P. Bordet,* S. Miraglia,* J. L. Hodeau,* and M. Marezio†

*Laboratoire de Cristallographie CNRS, BP166, 38042 Grenoble Cedex 9, France; and †MASPEC-CNR, Parco Area delle Scienze, 43100 Parma, Italy

Received December 30, 1998; in revised form May 13, 1999; accepted June 1, 1999

**To understand the competition between magnetic ordering and superconductivity at low temperature in $(Sn_{1-x}Er_x)(1)Er(2)_4Rh_6Sn(2)_{18}$ compounds the variation as function $x$ of the a.c. susceptibility and the magnetic structure, as determined by single-crystal neutron diffraction, were investigated. For increasing $x$, the low temperature properties change from coexistence of magnetic ordering and superconductivity ($x = 0$) to reentrant superconductivity ($x \approx 0.4$) and to magnetic ordering only ($x \approx 0.6$). The neutron diffraction experiments at low temperatures carried out for three samples of compositions $x = 0$, 0.42, and 0.6 allowed us to determine the variation of the low-temperature magnetic structure as a function of the mixed $(Sn_{1-x}Er_x)(1)$ site composition. Our results indicate that the changes in the low-temperature physical properties are essentially related to the increase in coherence length of the magnetic ordering for increasing $x$. For $x = 0$, only short-range magnetic order of the Er(2) sublattice is present, with a correlation length of only a few unit cells large. For the intermediate $x = 0.42$ sample, superconductivity appears and is suppressed at lower temperature due to magnetic ordering. For $x = 0.6$, long-range magnetic order is established for one of the two Er sublattices, preventing the appearance of superconductivity. This allows the coexistence of superconductivity and short-range magnetic order.** 

*Key Words:* **magnetism; superconductivity; erbium rhodium stannide.**

## INTRODUCTION

The compounds belonging to the rare-earth transition metal stannide series were synthesized for the first time in 1980 (1). From the physical property point of view, the main interesting feature of this series lies in the existence of superconductivity and/or magnetic ordering at low temperatures. The research effort devoted to these materials was essentially motivated by the study of the appearance of superconductivity in compounds containing a sublattice of magnetic rare-earth metal atoms. It was thought in the past that superconductivity and magnetism were two mutually incompatible cooperative phenomena. For example, Matthias *et al.* (2) showed that the introduction of magnetic impurities in a superconducting material led to the msuppression of superconductivity, or at least to a drastic decrease in the superconducting transition temperature. In the 1970s the first superconducting ternary compounds containing a sublattice of magnetic rare-earth metal atoms, such as $ErRh_4B_4$, or $HoMo_6S_8$, were discovered. It was shown in these materials that superconductivity was destroyed by the appearance of a ferromagnetic ordering.

Short after the discovery of the rare-earth transition metal stannide series, the reentrant superconductivity phenomenon was also observed in the erbium member with chemical formula $(Sn_{1-x}Er_x)(1)Er(2)_4Rh_6Sn(2)_{18}$, and extensive physical as well as crystallographic studies were devoted to the study of this peculiar effect (3–5). Furthermore, large single crystals were available for this compound, which allowed accurate physical characterizations and precise determination of the crystallographic and magnetic structures using neutron and X-ray single-crystal diffraction techniques. Ott *et al.* (4) showed that, depending on the synthesis conditions, the samples could behave differently. By measuring the low-temperature physical properties of three different single crystals, these authors observed for the first one only a superconducting transition, for the second only a magnetic ordering transition, and for the third two successive superconducting and magnetic transitions on cooling, characteristic of the reentrant behavior. Without the precise knowledge of both the crystal structure and the chemical composition of their samples, they were unable to explain their observations.

The crystal structure of this compound (known as phase II of the rare-earth transition metal stannides) was later determined by Hodeau *et al.* (6). The symmetry is tetragonal, space group $I4_1/acd$, with $a = 13.733$ Å, $c = 27.418$ Å, and $Z = 8$. The structural study led to the following chemical formula: $(Sn_{1-x}Er_x)(1)Er(2)_4Rh(1)_2Rh(2)_4Sn(2)_4Sn(3)_{12}Sn(4)_2$, where numbers in parentheses refer to different crystallographic sites in the unit cell. The framework of the structure is built up by a network of $RhSn_6$ trigonal prisms, to which only the Sn(2) and Sn(3) atoms contribute.



0022-4596/99 $30.00

It comprises layers of corner-sharing prisms with two successive layers being separated by a layer of isolated prisms. The prisms belonging to the separated prism layers share their corners only with those from the layers above and below. This three-dimensional network is represented in Fig. 1. It generates three types of large cavities centered at the 8*b* (0 0 1/4), 16*e*(1/4 $x \approx 1/4$ 1/8), and 8*a*(0 0 0) positions of the $I4_1/acd$ space group (with the origin taken at (0 1/4 − 1/8) from the center of symmetry), respectively. The 8*a* position remains empty, while the 8*b* one is occupied by Er(1) and Sn(1) atoms, in a slightly distorted cuboctahedral coordination of Sn(3) atoms. The 16*e* position is occupied by Sn(4) atoms, with two Er(2) atoms as first nearest neighbors, forming a doublet. The coordination polyhedron of these Er(2) atoms is a truncated cuboctahedron of 10 Sn atoms (average distance, 3.22 Å), three Rh atoms lying nearer (average distance, 3.03 Å) in front of the three rectangular faces of the Sn polyhedron.

The Er(2) sublattice is made of large distorted tetrahedra centered about the 8*a* positions, the Er(2)–Er(2) average distance being 5.28 Å. The above-mentioned doublets are formed by pairs of Er(2) atoms connecting two adjacent $Er(2)_4$ tetrahedra. The distance between two Er(2) atoms forming such doublets is 4.376 Å, shorter than the bond distance inside the tetrahedra. The $(Sn_{1-x}Er_x)(1)Er(2)_4$ sublattice, shown in Fig. 2, can be described as two interpenetrating pseudo-face centered cubic sublattices formed by the Er(2)4 tetrahedra and the $(Sn_{1-x}Er_x)(1)$ mixed sites, respectively.

For the compounds crystallizing in phase II, the *c*/*a* ratio is close to 2. Consequently, twinning by pseudo-merohedry is likely to occur about a pseudo threefold axis, leading to

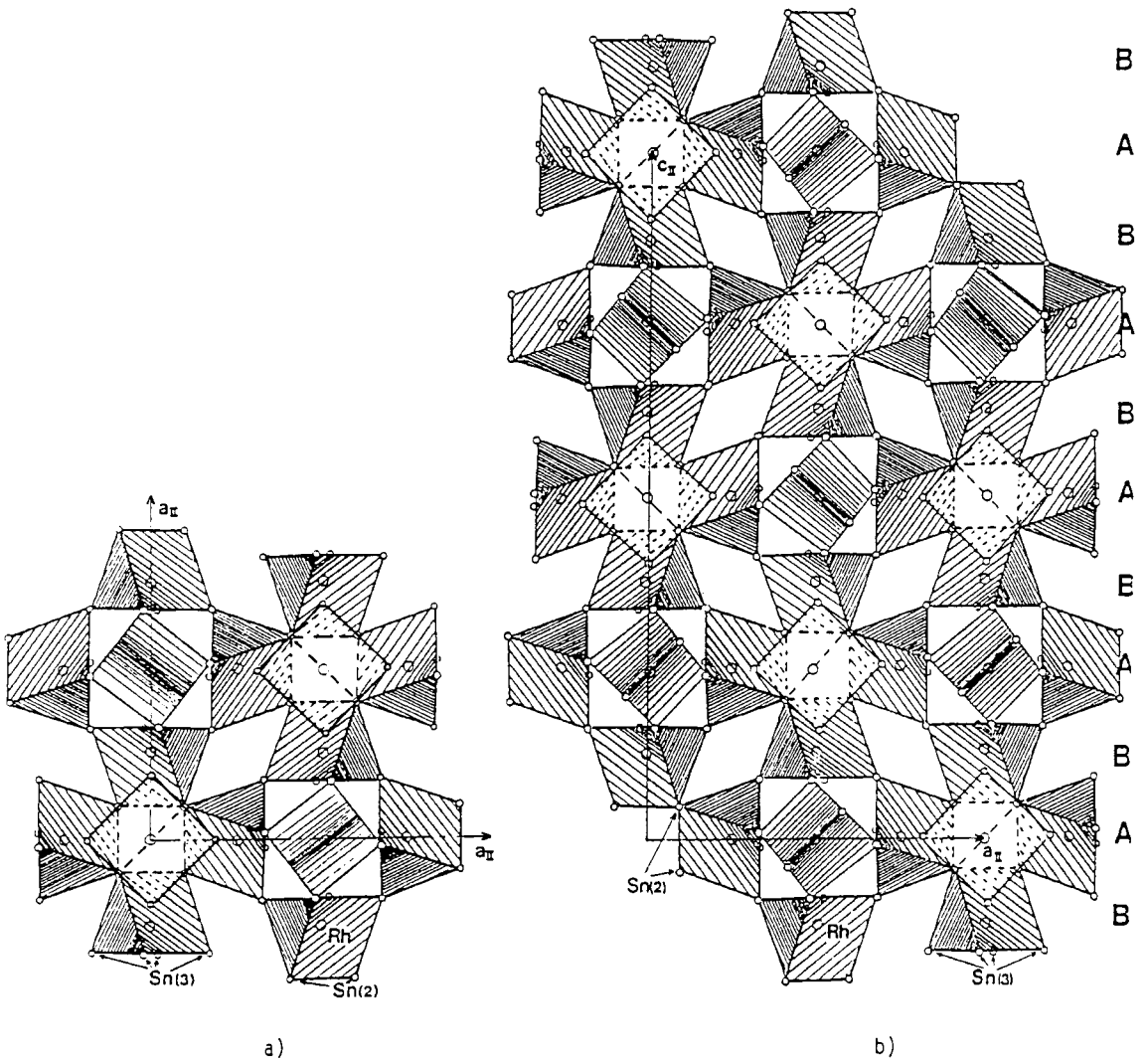


**FIG. 1.** Three-dimensional network of $RhSn_6$ trigonal prisms. Two successive A layers of corner-sharing prisms are separated by B layers of isolated prisms. (a) Projection on the (001) plane; (b) projection on the (100) plane.

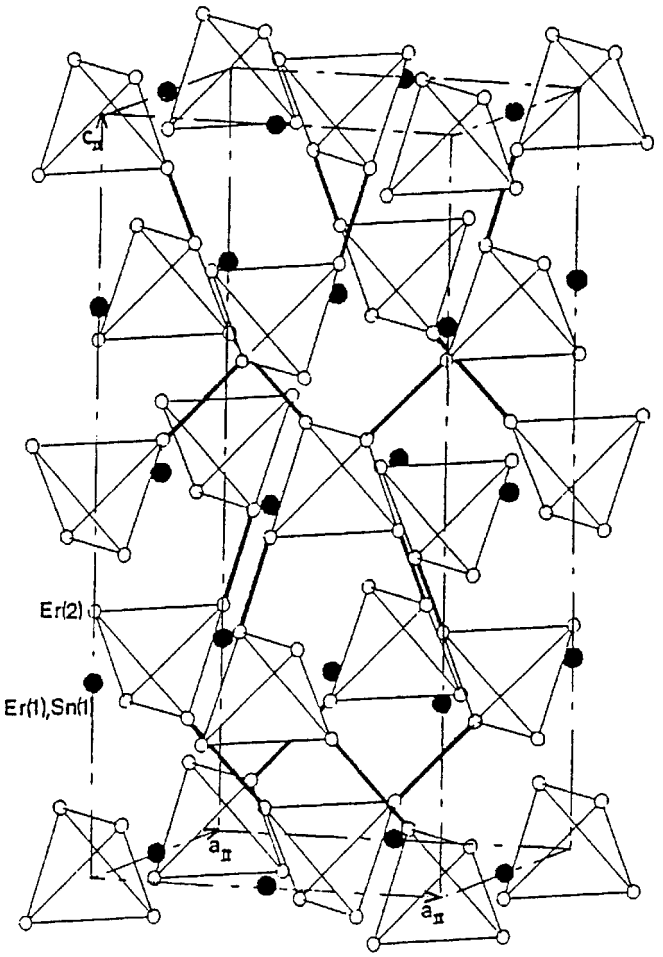


**FIG. 2.** Representation of the $(Sn_{1-x}Er_x)(1)$ (full circles) and Er(2) (empty circles) sublattices. The Er(2) doublets are outlined.

a $2a \times 2a \times c$ pseudo-cubic cell. The dimensions of the twin individuals change from sample to sample and have been estimated to vary between 1 and 100 μm.

By solving the structure of this compound, Hodeau *et al.* showed that the chemical composition could be varied by changing the composition of the mixed site $(Sn_{1-x}Er_x)(1)$. Miraglia *et al.* (7) then demonstrated that the three samples studied by Ott *et al.* presented different compositions of this site, with $x \approx 0.6$ for the magnetic sample, $x \approx 0$ for the superconducting one, and $x \approx 0.4$ for the reentrant one.

We present herein a detailed study of the chemical composition of selected samples of $(Sn_{1-x}Er_x)(1)Er(2)_4Rh_6Sn(2)_{18}$, the low-temperature properties, and the interplay between crystal and magnetic structures based on single-crystal neutron diffraction data at low temperature.

## SAMPLE PREPARATION

The samples used here were synthesized by using the tin melt technique (8, 9). A mixture of erbium, rhodium, and excess tin was heated at 1050°C in an evacuated quartz ampoule, then cooled down to 550°C at a rate varying between 3 and 25°C/h, and taken out of the furnace. Millimetric-size single crystals had metallic aspect and in general cuboctahedral shape. They were extracted from the melt by electrolysis. The precise chemical composition of each crystal was determined by single-crystal X-ray diffraction on a small piece of each sample (10).

## LOW-TEMPERATURE PHYSICAL MEASUREMENTS

A.c. susceptibility and magnetization measurements were carried out down to 10 mK at the C.R.T.B.T.-CNRS (Grenoble) in collaboration with J.L. Génicon and M. Giroud. In Fig. 3 the a.c. susceptibility curves for three samples of compositions $x = 0$, 0.41, 0.57, and 0.61 are shown (11). The evolution of the superconducting and magnetic transition temperatures are reported in Fig. 4. The $x = 0.61$ sample only presents a ferromagnetic transition at 0.64 K, and no trace of superconductivity. The $x = 0.57$ sample presents a superconducting transition at 0.97 K in a 3 mOe field. The superconducting state is quite fragile and is almost destroyed in a fiels as small as 300 mOe. The magnetic transition appears below $T_{m_{3\,mOe}} = 0.5$ K, which is accompanied by the disappearance of the superconducting state. Below this temperature, the magnetic state does not change with applied magnetic field. In the case of the $x = 0.41$ sample, the superconducting transition appears at $T_{c_{3\,mOe}} = 1.0$ K, and the superconducting state is merely sensitive to the increase of applied magnetic field. The ferromagnetic transition at $T_{m_{3\,mOe}} = 0.5$ K destroys the superconducting state. The magnetic state is sensitive to the increase in applied magnetic field, which increases the magnetic transition temperature as well as the maximum susceptibility value. Finally, in the case of the $x \approx 0$ sample, the superconducting transition takes place at $T_{c_{3\,mOe}} = 1.32$ K and the superconducting state is not affected by the applied magnetic field increase. A weak magnetic transition, whose magnitude is very sensitive to the applied magnetic field, appears at $T_{m_{3\,mOe}} = 0.34$ K. Nevertheless, the susceptibility remains diamagnetic below this temperature, indicating the coexistence between superconductivity and an ordered magnetic state for temperatures below 0.3 K.

The evolution of the transition temperatures as function of chemical composition ($x$) and applied magnetic field summarized in Fig. 4 indicates that an increase in $x$ at constant field leads to an increase in the magnetic transition temperature and a decrease in the superconducting transition temperature. Above $x = 0.6$ a further increase in $x$ leads to the suppression of the superconducting state. On the other hand, for constant $x$ value, $T_m$ increases and $T_c$ decreases with increasing applied magnetic field. These evolutions reveal a progressive weakening of the

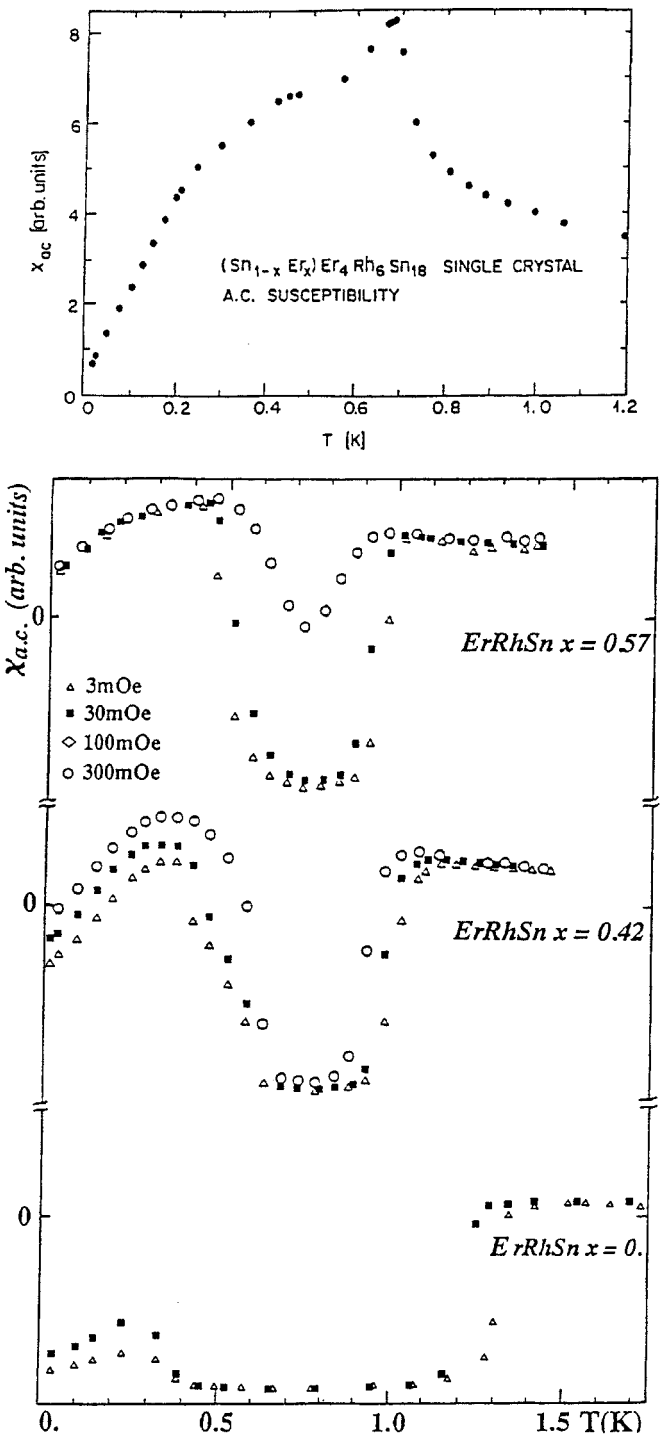


**FIG. 3.** Low temperature a.c. susceptibility curves for the $x = 0.61$ (top), $x = 0.57$, 0.42, and 0 (bottom).

superconducting state for increasing $x$ value and applied field, while the magnetic state is reinforced.

Magnetization and resistivity measurements at low temperature (12) on the $x = 0$ sample also revealed the existence of a ferromagnetic state below $T_m$, while the resistivity remains zero below a field of 20 mT. The saturation magnetization measurement leads to a value of 6.85 $\mu_B$ for the magnetic moment of the Er atoms. The coherence length of the superconducting state was estimated by Andres *et al.* (5) to be $\approx 1000$ Å. These results confirm the coexistence between ferromagnetic ordering and superconductivity with zero resistance below $T_m \approx 0.3$ K in the $x = 0$ compound.

## THE MAGNETIC STRUCTURE OF THE ERBIUM RHODIUM STANNIDE: EXPERIMENTAL

To understand the reentrant superconductivity phenomenon in erbium rhodium stannide, we decided to determine its magnetic structure. We carried out three single-crystal neutron diffraction experiments at low temperatures, with three samples having $x = 0.42$, 0.61, and 0, respectively, and whose physical properties have been described above. This would allow us to find out whether the modifications of these physical properties with the chemical composition of the $(Sn_{1-x}Er_x)(1)$ site were related to changes in the magnetic structure. The experiment was carried out using a dilution refrigerator installed on D15 of I.L.L., set in the normal beam geometry mode with a 1.17 Å wavelength. The preoriented samples were tin-soldered on a copper holder attached to the cryostat cold stage. They were centered in the neutron beam, and the crystal orientations were refined by measuring the position of 20 Bragg reflections.

To determine the twin ratios, several sets of equivalent reflections were measured for those reflections which do not belong to the $a \times a \times c/2$ pseudo-cubic subcell. This class of

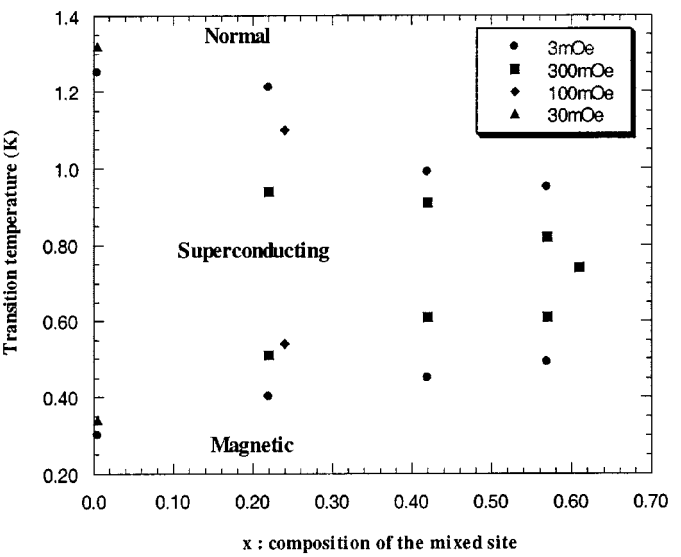


**FIG. 4.** Variation of the magnetic and superconducting transition temperatures as function of $x$ and applied magnetic field.

**TABLE 1**
**Atomic Positins at 2.5 K for the Compound $(Sn_{1-x}Er_x)(1)Er(2)_4\ Rh_6Sn(2)_{18}$, $x = 0.42$**

| Atom | Pos. | $x$ | $y$ | $z$ | Atom | Pos. | $x$ | $y$ | $z$ |
|---|---|---|---|---|---|---|---|---|---|
| Er/Sn(1) | 8*b* | 0 | 1/4 | 1/8 | Er(2) | 32*g* | 0.1327(8) | 0.388(1) | − 0.1933(5) |
| Sn(2) | 32*g* | 0.086(1) | 0.3387(8) | − 0.0800(6) | Sn(31) | 16*f* | 0.181(1) | 1/4 + $x$ | 1/8 |
| Sn(32) | 16*f* | 0.322(1) | 1/4 + $x$ | 1/8 | Sn(33) | 32*g* | 0.331(1) | 0.2591(1) | − 0.038(1) |
| Sn(34) | 32*g* | 0.005(1) | 575(1) | − 0.038(1) | Sn(4) | 16*e* | 0.230(3) | 0.465(1) | − 0.010(2) |
| Rh(1) | 16*d* | 0 | 0 | 0.001(1) | Rh(2) | 32*g* | 0.02420(9) | 0.2528(9) | − 0.1251(7) |

*Note.* Isotropic thermal parameters are fixed to 0. The value of $x$ is fixed at 0.42, as found by X-ray diffraction.

reflection belongs only to one twin individual. The ratios between the intensity of equivalent reflections were taken equal to the volume ratios of the twin individuals in the samples. For the three samples, two intensity data collections were carried out in the pseudo-cubic $2a \times 2a \times c$ supercell, above and below the magnetic transition temperature. This cell will be designated with subscript c, while the $a \times a \times c$ tetragonal cell will be designated with subscript t. The intensities of a few magnetic peaks were measured as function of temperature across the magnetic transition. The refinements were carried out with the MXD software (13). The twins and magnetic domains were taken into account by considering that each reflection was the weighted sum of reflections coming from the different individuals or domains. The weights were related to the individuals volume fractions, which were variable parameters.

## STUDY OF THE REENTRANT SUPERCONDUCTOR $(Sn_{1-x}Er_x)(1)Er(2)_4Rh_6Sn(2)_{18}$, $x = 0.42$

### *Crystal Structure at 2.5 K*

The refinement of the crystal structure was carried out on the intensities of 247 reflections measured at 2.5 K, with a weighting scheme $w = 1/(\sigma + 0.02I_{obs})^2$. An absorption correction was applied, using the Cooper and Rouse formula (14) for a sphere and $\mu R = 0.15$. All positional parameters and twin ratios were refined while the isotropic thermal factors were fixed to zero. The compositional $x$ parameter was taken equal to the 0.42 as determined by X-ray diffraction analysis. The final reliability factors were w$R = 10.17\%$, $R = 7.2\%$, and $X^2 = 2.15$. The refined twin ratios (38.1(6)%, 34.4(6)%, and 25.5(6)%) were in good agreement with those determined from the intensity ratios of equivalent reflections as described above. The refinement of the isotropic thermal parameters yielded values equal to zero within two standard deviations and did not modify the other results. The atomic positions obtained at 2.5 K are reported in Table 1. They hardly differ from those of the room temperature crystal structure reported by Hodeau *et al.* (6).

### *Magnetic Structure at 70 mK*

The thermal evolution of the $(4\,4\,8)_c$ reflection intensity is shown in Fig. 5. The nuclear part of this intensity is the sum of the $(2\,2\,8)_t$, $(4\,2\,4)_t$, and $(2\,4\,4)_t$ reflections from the three twin individuals. The magnetic transition temperature taken at the inflection point is estimated at 0.35 K.

By subtracting the intensities measured below and above the transition, it appeared that only about 30 reflections presented a nonnegligible magnetic contribution. Almost all of them were indexable on the pseudo-cubic $a \times a \times c/2$ body-centered cell. Since the phase II structure unit cell contains 32 Er(2) and 8 $(Sn_{1-x}Er_x)(1)$ sites, it was not possible to refine independently the moduli and directions of all magnetic moments. Therefore, we used the Bertaut's macroscopic theory (15) by imposing on the magnetic moments the restrictions brought about by symmetry conditions. For each representation of the space group, a set of relations constraining the moduli and directions of the Er magnetic moments on crystallographically equivalent sites were applied. The remaining independent variables describing the magnetic moments were refined, while the positional

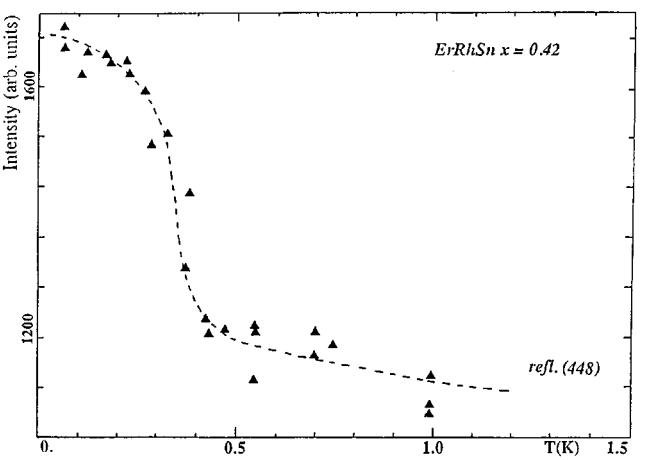


**FIG. 5.** Intensity variation with $T$ for the $(4\,4\,8)_c$ reflection across the magnetic transition for $x = 0.42$.

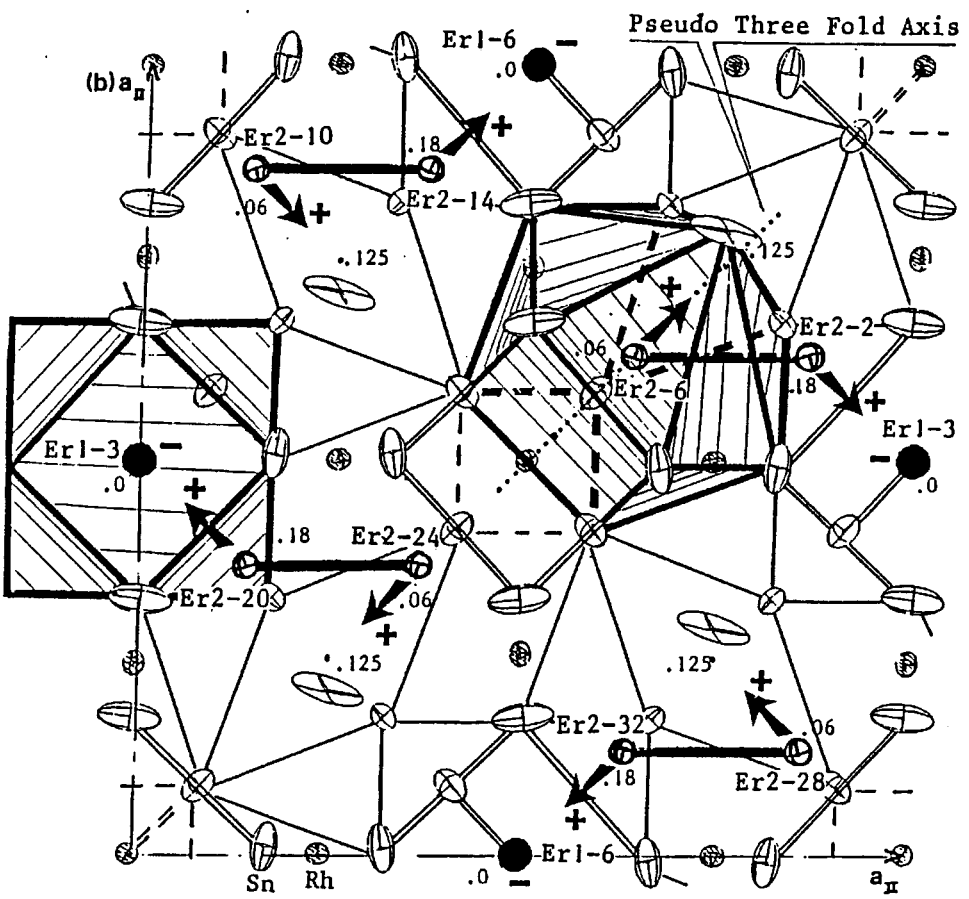


**FIG. 6.** Projection on the (001) plane for atoms with $-0.05 < z < 0.21$. The dotted line indicates the local pseudo threefold axis at the Er(2) site. The Er(2) moments are indicated by arrows. The + and − signs indicate the direction of the Er(1) moments along the $c$ axis.

parameters, twin ratios, and scale factors were fixed at the values determined at 2.5 K. All representations for the $I4_1/acd$ space group were tested, and satisfactory convergence could only be obtained for the $\Gamma^{2+}$ one (16, 17). In this representation, the Er(1) magnetic moments have the same direction parallel to the $c$ axis of the $a \times a \times c$ tetragonal cell. The Er(2) moments are not collinear, and have a resultant parallel to the $c$ axis. The magnetic moments of the Er(2) atoms were described in polar coordinates, with the cartesian coordinates $Mx$, $My$, $Mz$ given by

$$Mx = \mu\mathrm{Er}(2)\sin\varphi\cos\chi$$

$$My = \mu\mathrm{Er}(2)\sin\varphi\sin\chi$$

$$Mz = \mu\mathrm{Er}(2)\cos\varphi.$$

The refined variables were $\mu$Er(1), $\mu$Er(2), $\varphi$, and $\chi$. Since the sample was not submitted to external field during the experiment, the presence of magnetic domains had to be introduced in the refinement. Since for the $\Gamma^{2+}$ representation the resulting magnetic moment is oriented along the $c$-axis, three domains, related by the pseudo-threefold axis of the $a \times a \times c/2$ cell, were introduced.

The refinement carried out on the total (nuclear + magnetic) intensities yielded $\mu\mathrm{Er}(1) = 3.9(5)\,\mu_B$, $\mu\mathrm{Er}(2) = 1.5(1)\,\mu_B$, $\chi = 37(10)^\circ$, and $\varphi = 301(4)^\circ$, with the following reliability factors: w$R = 13.26\%$, $R = 7.02\%$, and $X^2 = 3.32$. A refinement carried out on the intensity differences between 70 mK and 2.5 K (i.e., only the magnetic contributions) led to the same results within one e.s.d. The values of the Er magnetic moments are markedly less than those obtained by Mössbauer spectroscopy (7.6 $\mu_B$) (3) or magnetization measurements (8.13 $\mu_B$) (5) on reentrant samples with unknown composition.

The projection onto the (001) plane of the magnetic and crystallographic structure is presented in Fig. 6. One can see that the orientation of the Er(2) atom moment is close to the direction of the pseudo-threefold axis passing through the Er(2) site, for which $\chi = 45^\circ$ and $\varphi = 305.26^\circ$. Refining the magnetic moment moduli with $\chi$ and $\varphi$ fixed at these values led to similar results as above. It can then be stated that the

magnetic moments of the Er(2) atoms are oriented along the local pseudo-threefold axis.

The magnetic structure of the Er sublattices is presented in Fig. 7. Inside each $Er(2)_4$ tetrahedron, the magnetic moments of the four Er(2) atoms are oriented along the four pseudo-threefold axes, with a resultant along the $c$ axis having a direction opposite to that of the Er(1) sublattice magnetic moments. The total magnetic moment per unit cell is 14(5) $\mu_B$ and is directed along the $c$ axis.

The observed magnetic contributions to the Bragg peaks always exhibited a full width at half maximum (FWHM) markedly larger than that of the nuclear contribution. For example, Fig. 8 shows the fitted profiles of the $(4\,4\,8)_c$ reflection at 0.7 K and 70 mK (above and below $T_m$), as well as the fitted profile of the difference, corresponding to the magnetic contribution only. Using the Scherrer formula, and considering the FWHM of the Bragg contribution as the instrumental width, the coherence length of the magnetic ordering can be estimated at about 65 Å.

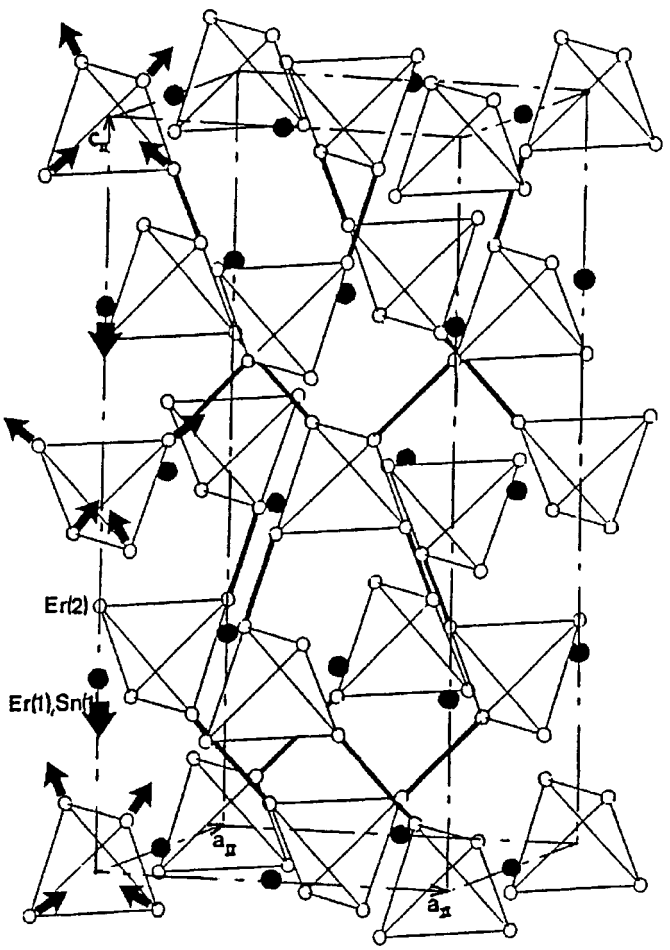


**FIG. 7.** Orientations of the magnetic moments for the two Er(1) and Er(2) sublattices.

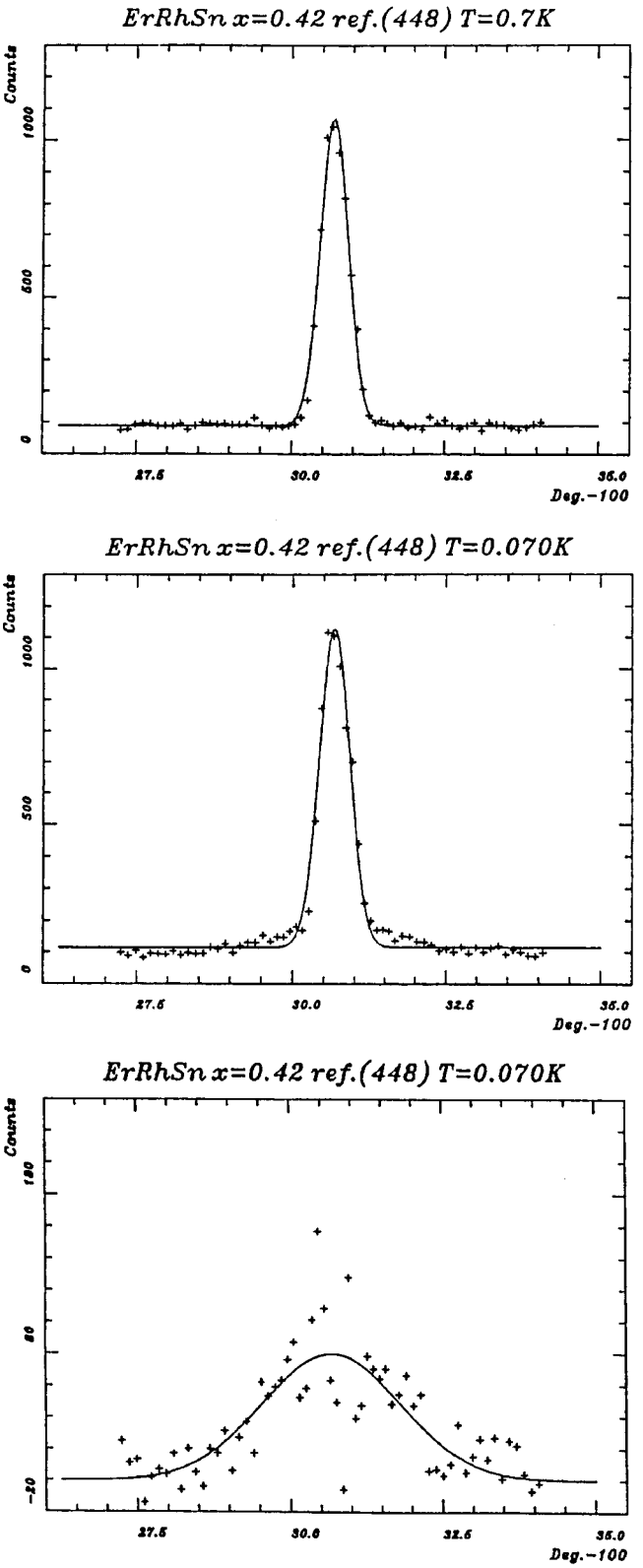


**FIG. 8.** Profile fitting for the $(00\text{-}8)_c$ reflection ($x = 0.42$). From top to bottom: above, below the magnetic transition, and difference between the two.

### STUDY OF $(Sn_{1-x}Er_x)(1)Er(2)_4Rh_6Sn(2)_{18}$ WITH $x = 0.61$

Figure 9 represents the thermal evolution of the $(8\,4\,4)_c$, $(0\,0\,8)_c$, and $(2\,2\,2)_t$ reflections across the magnetic transition. The transition temperature taken at the inflection point is 0.4 K. Two data collections have been carried out at 1.4 K and 100 mK, under the same conditions as described above for the $x = 0.42$ sample. The refinements of the nuclear and magnetic structures also yielded similar results, with $\mu Er(1) = 2.4(2)\,\mu_B$ and $\mu Er(2) = 3.65(9)\,\mu_B$, corresponding to an increase of $\approx 2\mu_B$ of the Er(2) magnetic moment. The magnetic resultant per unit cell is $34(3)\,\mu_B$, directed along the $c$ axis.

As for the reentrant compound, the magnetic contributions are noticeably broader than the nuclear ones. The results of profile fittings for the $(0\,0\,8)_c$ reflection are shown in Fig. 10. Interestingly, the purely magnetic contribution obtained by the difference between the reflections measured below and above the transition must also be fitted with two Gaussian components with FWHM 0.27(1)° and 1.04(5)°, respectively, while the nuclear contribution exhibits a FWHM of 0.264(5)°. These two magnetic contributions could be attributed to the two magnetic sublattices present in the structure. The FWHM of the narrow one is similar to the FWHM of the nuclear contribution, and therefore corresponds to a long-range ordered magnetic sublattice. The FWHM of the broad one corresponds to a magnetic coherence length of $\approx 60$ Å, very close to the value found for the reentrant sample. Thus, in this compound, two magnetic sublattices coexist, one being long-range ordered and the other being short-range ordered with a coherence length of the order of a few unit cells.

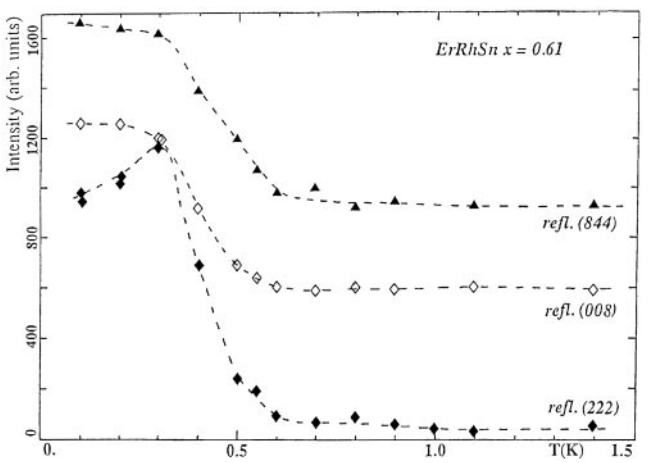


**FIG. 9.** Intensity variation with $T$ for the $(8\,4\,4)_c$, $(0\,0\,8)_c$, and $(2\,2\,2)_c$ reflections across the magnetic transition for $x = 0.61$

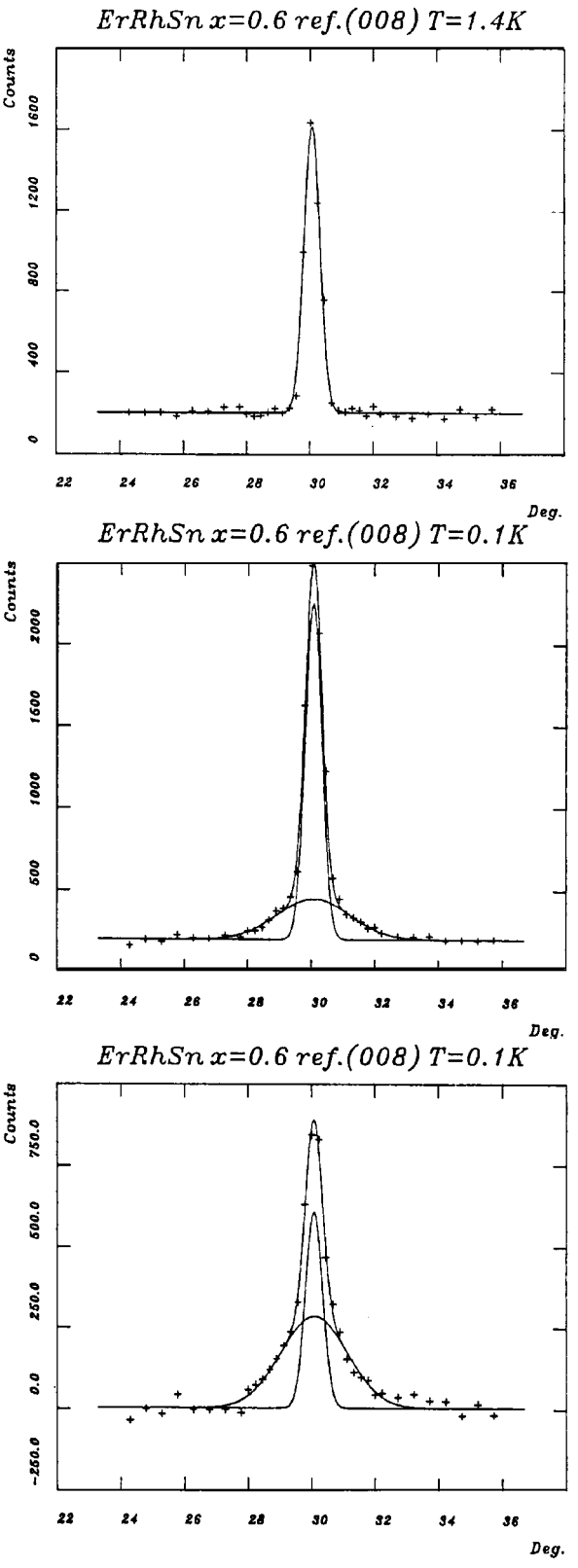


**FIG. 10.** Profile fitting for the $(008)_c$ reflection ($x = 0.61$). From top to bottom: above, below the magnetic transition, and difference between the two.

### STUDY OF $Sn(1)Er(2)_4Rh_6Sn(2)_{18}$ WITH ($x = 0$)

Figure 11 shows the thermal evolution of the $(4\,4\,-8)_c$, $(0\,0\,8)_c$, and $(2\,2\,-2)_c$ across the magnetic transition. The transition temperature taken at the inflection point is 0.35 K. Note that this compound is still superconducting below this temperature which confirms the coexistence of magnetic ordering and superconductivity in this sample. The refinement of the nuclear and magnetic structures from the 2.5 K and 85 mK data leads again to results similar to both previous samples, with the difference being that in this case only the Er(2) sublattice was introduced in the magnetic structure refinement, which yielded $\mu Er(2) = 2.28(8)\ \mu_B$. The magnetic resultant per unit cell is $32(4)\ \mu_B$ and is directed along the $c$ axis. This high value compared to the one found for the reentrant sample is due to the fact that the contribution from the Er(2) sublattice is no longer partly compensated by the contribution from the Er(1) one.

As for the other two samples, the magnetic contribution to the Bragg peaks showed noticeable broadening. The profile fits for the $(0\,0\,8)_c$ reflection is shown in Fig. 12. The nuclear peak at 2.0 K is described by a Gaussian curve with FWHM = 0.245(8)°, while for the magnetic contribution, a FWHM of 1.7(2)° is obtained, corresponding to a quite short correlation length of $\approx 40$ Å.

### DISCUSSION

Our results indicate that for the sample with $x = 0$ the magnetic order is established with coherence lengths on the order of a few unit cells and consequently does not destroy the superconducting state. The short-range nature of the magnetic order cannot be attributed to structural disorder on site (1), since it is only occupied by Sn atoms. It should be related, instead, to the arrangement of the Er(2) sublattice.

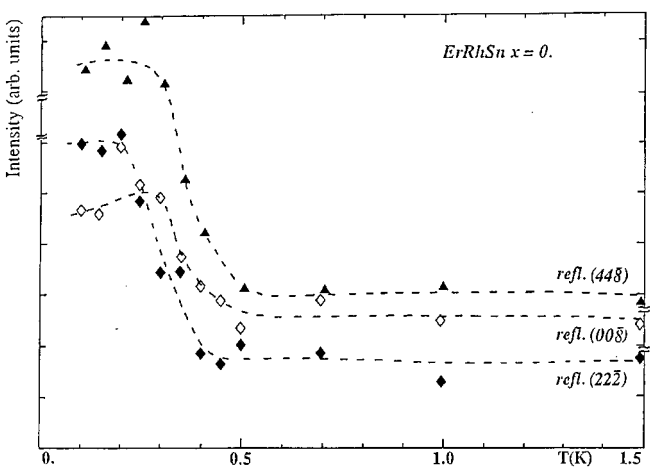


**FIG. 11.** Intensity variation with $T$ for the $(4\,4\,-8)_c$, $(0\,0\,-8)_c$, and $(2\,2\,-2)_c$ reflections across the magnetic transition for $x = 0$.

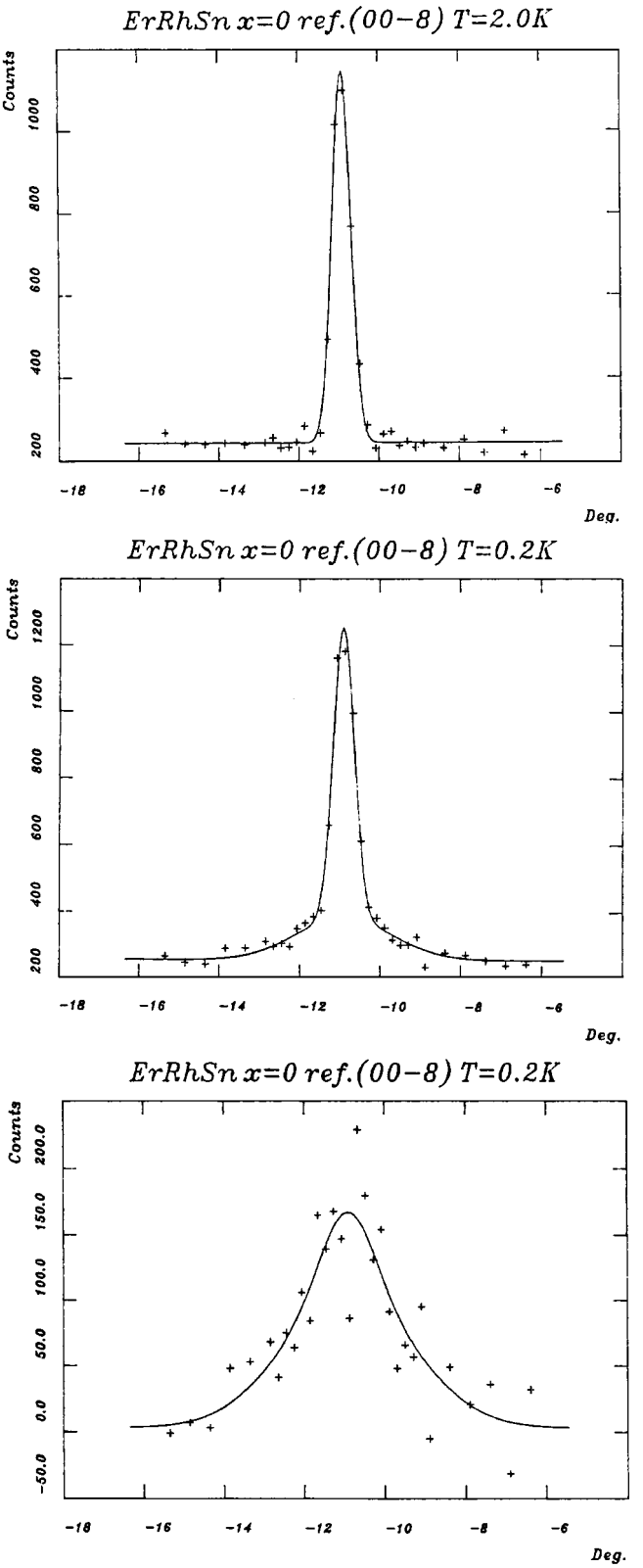


**FIG. 12.** Profile fitting for the $(00\,-8)_c$ reflection ($x = 0$). From top to bottom: above, below the magnetic transition, and difference between the two.

It is interesting to note that a spin glass behavior has been reported by Blank *et al.* (18) for erbium rhodium stannide and by Lazaro *et al.* (19) and van de Pasch (20) for isostructural holmium rhodium stannide. These observations and the short-range nature of the magnetic ordering for $x = 0$ suggest that the erbium rhodium stannide could be a spin glass system even in the absence of the structural disorder on site (1). Since the Er(2) sublattice is pseudo-cubic, the magnetic resultant can be oriented along the three major unit cell directions leading to the formation of magnetic domains of sizes corresponding to the coherence length determined by neutron diffraction experiments. The presence of such microdomains could be generated by structural defects of the same type as those which are systematically observed in phase II', a microtwinned and disordered version of phase II (20). It is known that the erbium rhodium stannide can crystallize in either of these two phases. It is thus highly probable that a nonnegligible number of such defects may exist in phase II samples, leading to a disorder of the magnetic Er(2) sublattice. Magnetic frustration related to the different possible orientations of the magnetic resultant in the vicinity of such defects could be at the origin of the spin glass behavior of the system.

For $x > 0$, Er atoms are present on site (1). For sufficiently high occupancy of this site by Er ($x = 0.6$), the neutron diffraction data revealed the presence of two magnetic contributions, one long-range ordered and the other short-range ordered, which can be attributed to the two magnetic sublattices. It is difficult to imagine that the short-range ordered sublattice be that of Er(2), as in the case of the $x = 0$ sample. It is unlikely that the magnetic orientation disorder of this sublattice would coexist with the long-range ordering of the Er(1) sublattice. The orientation of the Er(1) moments along the *c* axis direction suggests that the crystal-field effects should play a relevant role in this case. The presence of magnetic moments on the Er(1) sublattice could lead to an increase in the size of magnetic domains, which would become larger than the diffraction correlation length (about a few hundred Å) for $x = 0.6$. The Er(2) sublattice would then appear as long-range ordered, while the short range contribution to the magnetic diffraction peaks would be brought about by the substitutionally disordered Er(1) sublattice. For the $x = 0.42$ sample, the effect of the Er(1) moments would be insufficient to lead to long-range ordering of the Er(2) sublattice, both types of disorder would be present, leading to the observation of a single, broad magnetic contribution to the Bragg reflections.

The coexistence of magnetic ordering and superconductivity in the $x = 0$ sample could be explained by the short-range nature of the former, for which the magnetic correlation length ($\approx 40$ Å) is considerably smaller than the superconducting coherence length, known to be about $\approx 1000$ Å. The net magnetic field, resulting from averaging over many small magnetic domains of such dimensions, would probably be close to zero. The a.c. susceptibility behavior observed below $T_m$ would result from the superposition of the dimagnetic signal due to superconductivity and the ferromagnetic signal due to short-range magnetic ordering.

When $x$ increases, the magnetic correlation length decreases, and the magnetic field is established over larger distances. Despite the decrease in the resulting magnetic moment per unit cell, the increase in the correlation length leads to the disappearance of superconductivity, whose critical field Hc2 is only $\approx 100$ Oe. The material is now a reentrant superconductor. However, superconducting islands might remain below $T_m$, which might explain the dependence of a.c. susceptibility with applied magnetic field. An increase in the applied field would lead to an increase in the magnetic correlation length, which would contribute to the decrease in the superconducting islands. For $w \approx 0.6$, the magnetic coupling is strong enough to lead to long-range magnetic ordering of the Er(2) sublattice. The resulting increase in magnetic transition temperature prevents the appearance of superconductivity in this sample. The coherence length of the Er(2) sublattice is increased by increasing the proportion of magnetic erbium cations in the mixed site (1).

## CONCLUSION

The magnetic structure of the erbium rhodium stannide has been investigated as a function of the mixed site composition $x$ by means of very low temperature single-crystal neutron diffraction. Our results indicate that the changes in the low-temperature physical properties are essentially related to the increase in coherence length of the magnetic ordering for increasing $x$. For $x = 0$, only short-range magnetic order of the Er(2) sublattice is present with a correlation length of only a few unit cells large. For the intermediate $x = 0.42$ sample, superconductivity appears and is suppressed at lower temperature due to magnetic ordering. For $x = 0.6$, long-range magnetic order is established for one of the two Er sublattices, presenting the appearance of superconductivity. The coherence length of the Er(2) sublattice is increased by increasing the proportion of magnetic erbium cations on the mixed site (1).

In this system, the complex competition between magnetism and superconductivity appears to be governed by the relative sizes of the magnetic and superconducting coherence lengths. On increasing the former by progressively increasing the erbium occupancy of site (1), the superconducting state is weakened and confined to small domains, before disappearing for sufficiently high erbium concentration and magnetic coherence length.

## ACKNOWLEDGMENTS

The authors thank P. Chaudouet and F. Weiss (L.M.G.P. Grenoble) for sample preparation, M. Giroud and J. L. Génicon (C.R.T.B.T. CNRS

Grenoble) for low temperature measurements, and J. L. Ragazzoni and P. J. Brown (I.L.L.) for their help during the neutron diffraction experiments.

## REFERENCES

1. J. P. Remeika, G. P. Espinosa, A. S. Cooper, H. Barz, J. M. Rowell, D. B. McWhan, J. M. Vandenberg, D. E. Moncton, Z. Fisk, L. D. Woolf, H. C. Hamaker, M. B. Maple, G. Shirane, and W. Thomlinson, *Solid State Commun.* **34,** 923 (1980).
2. B. T. Matthias, H. Suhl, and E. Corenzwit, *Phys. Rev. Lett.* **1,** 92 (1959).
3. G. K. Shenoy, F. Probst, J. D. Cashion, P. J. Viccaro, D. Niarchos, B. D. Dunlap, and J. P. Remeika, *Solid State Commun.* **37,** 53 (1980).
4. H. R. Ott, W. Odoni, Z. Fisk, and J. P. Remeika, *in* "Ternary Superconductors," p. 251, North Holland, Amsterdam, 1981.
5. K. Andres, J. P. Remeika, G. P. Espinosa, and A. S. Cooper, *Phys. Rev. B* **23,** 1179 (1981).
6. J. L. Hodeau, M. Marezio, and J. P. Remeika, *Acta Crystallogr. B* **40,** 26 (1984).
7. S. Miraglia, J. L. Hodeau, M. Marezio, H. R. Ott, and J. P. Remeika, *Solid State Commun.* **52,** 135 (1984).
8. G. P. Espinosa, A. S. Cooper, and H. Barz, *Mater. Res. Bull.* **17,** 963 (1982).
9. F. Weiss, S. El Fassi, D. Boursier, P. Bordet, and J. L. Hodeau, "Compte Rendu de la Réunion de la R.C.P. "Magnétisme, Liquide de Fermi, Supraconductivité," 14–17 Oct. 1985," Rencurel en Vercors.
10. P. Bordet, Thèse d'Etat, Univ. J. F.-Grenoble, 1989.
11. P. Bordet, J. L. Hodeau, P. Wolfers, J. L. Ragazzoni, J. L. Génicon, R. Tournier, P. Chaudouet, F. Weiss, G. Espinoza, and M. Marezio, *J. Phys.* **49,** C8-401 (1988).
12. M. Giroud, Thesis, Univ. J. F.-Grenoble, 1987.
13. P. Wolfers, *J. Appl. Crystallogr.* **23,** 554 (1990).
14. K. D. Rouse, M. J. Cooper, E. S. York, and A. Chakera, *Acta Crystallogr. A* **26,** 682 (1970).
15. E. F. Bertaut, *in* "Magtnetism" (G. T. Rado and H. Suhl, Eds.), Vol. III, p. 149, Academic Press, New York, 1963.
16. J. L. Hodeau, P. Bordet, P. Wolfers, M. Marezio, and J. P. Remeika, *J. Magn. Magn. Mater.* **54–57,** 1527 (1986).
17. P. Bordet, J. L. Hodeau, P. Wolfers, S. Miraglia, A. Benoit, M. Marezio, and J. P. Remeika, *Physica B* **136,** 432 (1986).
18. D. H. A. Blank and J. Flokstra, *Jpn. J. Appl. Phys. Suppl.* **26-3,** 1289 (1987).
19. F. J. Lazaro, A. M. van de Pasch, and J. Flokstra, *J. Magn. Magn. Mater.* **71,** 10 (1987).
20. A. M. van de Pasch, Thesis, Univ. Twente, The Netherlands, 1988.